Facile one-pot ultrasound-assisted solvothermal fabrication of ball-flowerlike nanostructured $(BiOBr)_x(Bi_7O_9I_3)_{1-x}$ solid-solution for high active photodegradation of antibiotic levofloxacin under sun-light

Shalaleh Gholizadeh Fard[a,b], Mohammad Haghighi[a,b,*,1], Maryam Shabani[a,b]

[a] Chemical Engineering Faculty, Sahand University of Technology, P.O.Box 51335-1996, Sahand New Town, Tabriz, Iran
[b] Reactor and Catalysis Research Center (RCRC), Sahand University of Technology, P.O.Box 51335-1996, Sahand New Town, Tabriz, Iran

ABSTRACT

Herein, the novel solid solution $(BiOBr)_x(Bi_7O_9I_3)_{1-x}$ nanophotocatalysts with different x values (x = 0, 0.25, 0.5, 0.75 and 1) have been synthesized with an one-pot sono-solvothermal method to degrade the antibiotic levofloxacin, as an emerging pollutant, under simulated solar light. Moreover, to investigate the effect of microjets energy produced from ultrasound, the solid solution $(BiOBr)_x(Bi_7O_9I_3)_{1-x}$, with optimum x, has been prepared using the one-pot solvothermal route. Synthesized products have been characterized by XRD, FESEM, HRTEM, EDX, BET-BJH, FTIR, DRS and pHpzc. It was found that $(BiOBr)_{0.75}(Bi_7O_9I_3)_{0.25}$-U fabricated with the presence of ultrasound had the highest percentage in the 50 mg/L levofloxacin degradation, which was 95.4%. This result was assigned to its high activation in the solar spectrum range due to the band gap at around 2.43 eV, more effective charge transportation and separations, decrease in the recombination rate, large specific surface area (125.3 m^2/g), great total pore volume (0.589 cm^3/g) and also uniform dispersion and increased nucleation owing to the presence of ultrasound energy, which has led to an increase in the catalytic active sites. Also operational parameters such as the photocatalyst loading, concentrations of pollutant and pH of solution were investigated. Furthermore, the reaction mechanism was suggested for levofloxacin photodegradation.

1. Introduction

The presence of pharmaceutical pollutants, as an emerging pollutant in the surface waters and underground waters can have destructive effects due to their high environmental stability, high toxicity and high resistance. So, the removal of these pollutants is considered necessary [1–3]. Among the consumable medicines, antibiotics are known to be the most widely used drugs [4,5]. In 2012, the total amount of antibiotics that consumed in the United States was 17,900 tons and also this amount was 162,000 tons for China, in 2013. These antibiotics include amoxicillin, co-amoxiclav, ofloxacin, ciprofloxacin, levofloxacin, metronidazole, azithromycin and tetracycline [6]. It should be noted that, depending on the type, amount of consumption and treatment methods that used, different concentrations for the drugs are mentioned in various waste water and aqueous solutions. The amount of fluoroquinolone such as amoxicillin, ciprofloxacin, ofloxacin and acetaminophen in some pharmaceutical effluents was reported to be 56, 14, 25.5 and 39 mg /L, respectively. 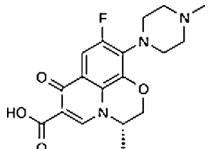Generally, the average concentration of the fluoroquinolone pollutants in the wastewater is about 40 mg/L [7–10]. Amongst the existing antibiotics, levofloxacin (LVO) can be used as a commonly used fluoroquinolone to treat many diseases such as prescribing for the treatment of many infectious diseases [11,12]. Herein our aim is post-treatment of wastewater so we have investigated the concentration of 50 mg /L levofloxacin antibiotic, because the amount of this pollutant in the environment increases over time. In Table 1, the physicochemical properties of levofloxacin antibiotic are presented.

Currently, one of the proposed methods for the elimination of the recalcitrant pollutants is the use of advanced oxidation processes (AOPs) [13–15]. Among the advanced oxidation processes, the photocatalytic process is considered as an appropriate choice for reasons such as process performance at ambient temperature and pressure, economic efficiency because of the solar energy utilization, low amounts of toxic by-products, increasing the amount of the mineralization of pollutants and high efficiency at low concentrations of photocatalyst [16–18]. In the recent decades, various photocatalysts such as CdS, TiO$_2$, ZnO,

Table 1
Physicochemical properties of Levofloxacin antibiotic.

Antibiotic	Chemical Formula	Chemical Structure	Molecular Weight (g/mol)	Solubility in Water (mg/mL)	λ_{max} (nm)
Levofloxacin	$C_{18}H_{20}FN_3O_4$		361.4	Water-soluble	287

Fe$_2$O$_3$, and WO$_3$ have been used for photocatalytic processes [19–21]. Among these, TiO$_2$ and ZnO have been very much considered due to their high optical and chemical stability, being non-toxic and cost- effective [22]. Despite the desirable properties, the use of these photocatalysts is limited due to the poor absorption of the visible light, wide band gap and high recombination rate of electron-hole pairs [23–25]. Recently, researches on photocatalysts are focused on new semiconductors with a smaller band gap that are active in the visible light range [26–28].

The group of photocatalysts, which could represent the good activity under visible light, is bismuth based photocatalysts. The appropriate band gap energy of these photocatalysts effectively affects the absorption of light. In addition, the high ionic conductivity, diverse morphology and proper surface area of the bismuth-based compounds make them as a suitable option for photocatalytic processes. To date, various bismuth based photocatalysts such as BiVO$_4$, BiOX, Bi$_2$O$_3$, Bi$_2$MoO$_6$ and Bi$_2$WO$_6$ have been discussed and studied, that among them, the bismuth oxyhalides (BiOX; X: Cl, Br, I) present the better performance due to their unique structure [29].

Bismuth oxyhalides have a tetragonal crystalline structure in which each of the cationic layers of [Bi$_2$O$_2$] is surrounded by two layers of halogen anionic atoms and formed the layers of [X-Bi-O-Bi-X].This structure can create an internal electric field that is very effective in the separation of the electron-hole that created during the photocatalytic reaction [30]. In addition, these photocatalysts have a specific electron structure and have 6 s and 2p orbitals in their capacity layer, while TiO$_2$ has only 2p orbital in its capacity layer. This particular electron structure leads to high activity, the mobility and effective separation of charge carriers and, consequently, the reduction of the recombination rate [16,31].

Researches have shown that among the bismuth oxyhalides, BiOBr has unique photocatalytic properties [32]. This photocatalyst have good activity because of its unique layer structure. But the light absorption and photocatalytic activity of this photocatalyst is low due to the band gap of 2.76 eV and the high recombination rate of electron-hole pairs [33–35]. One of the solutions to these challenges is to create a solid solution with other photocatalysts [36]. In this regard, the solid solutions such as BiOBr$_x$Cl$_{1-x}$ [37] and BiOBr$_x$I$_{1-x}$ [38] were synthesized and their performance were evaluated. The possibility of band gap adjustment of synthesized photocatalysts [39], an appropriate separation of the electron-hole and the reduction in the recombination rate due to the specific layered structure of these photocatalysts are the important advantages of this approach [40,41].

Solvothermal method due to the being low cost, simplicity of process equipment, controllability of operating conditions and thus the possibility of control of morphology is the most appropriate and most widely used method [42]. Furthermore, the use of ultrasonic waves during synthesis can have a significant effect on nucleation and uniform dispersion of phases. This event will definitely affect the growth of crystals and their sizes, as well as the effective dispersion of active sites and increased access to active sites, which can improve the performance of the photocatalytic process.

The main purposes of this research were: (i) synthesis of

(BiOBr)$_x$(Bi$_7$O$_9$I$_3$)$_{1-x}$ solid solution nanophotocatalyst with sono-solvothermal method; (ii) evaluation the effect of ultrasonic waves on the distribution of particles and nucleation and consequently in pollutant removal percentage; (iii) evaluation the effect of x on the physical and chemical properties and so on the degradation of antibiotic contaminants under simulated solar light; (iv) the investigation of photodegradation of antibiotic levofloxacin under simulated solar-light by the (BiOBr)$_x$(Bi$_7$O$_9$I$_3$)$_{1-x}$ solid solution nanophotocatalyst.

2. Materials and methods

2.1. Materials

All the chemical reagents that used in this study were analytical grade without extra purification. All over this study we used deionized water. For synthesizing nanophotocatalysts, Bi(NO$_3$).5H$_2$O, KI and KBr used as precursors of BiOBr and Bi$_7$O$_9$I$_3$, which Bi(NO$_3$).5H$_2$O was purchased from Sigma-Aldrich Company and KI and KBr were purchased from Merck Company. Also ethylene glycol used as a solvent that was obtained from Arman Sina Company.

2.2. Nanophotocatalysts preparation and procedure

As shown in Fig. 1S, the fabrication of nanophotocatalysts consists of three steps. Firstly, the preparation of the precursors is performed so that, in the synthesis of each sample, according to the amount of x in the (BiOBr)$_x$(Bi$_7$O$_9$I$_3$)$_{1-x}$ nanophotocatalysts, certain ratio of the precursors were prepared then firstly, Bi(NO$_3$).5H$_2$O was dispersed in 50 mL ethylene glycol by sonication in ultrasonic equipment (Ultrasonic Homogenizer, Ultrasonic Technology Development Co., Iran) for 1 h with a power of 200 W (Solution A). Simultaneously, KI and KBr were magnetically stirred in 20 mL ethylene glycol for 30 min (Solution B). In the next step, the solution B was added dropwise to the solution A during stirring, then the obtained solution sonicated by ultrasound radiations with a power of 200 W for 1 h to attain uniform distribution and increasing nucleation. The solvothermal synthesis was done in a 100 ml Teflon-lined stainless steel autoclave for 12 h at 150 °C. After completing the synthesis process, we waited until the autoclave cooled to room temperature. The third step, which is the last step, is the nanophotocatalysts post treatment. In this stage firstly the precipitate generated was filtered and then washed three times with deionized water. Afterward, the products obtained were dried at 110 °C for 12 h in air ambient. It is worth noting that, for studying the effect of ultrasonic waves, (BiOBr)$_{0.75}$(Bi$_7$O$_9$I$_3$)$_{0.25}$ nanophotocatalyst was synthesized in the same way without the use of ultrasonic waves. So that the solution was magnetically stirred instead of using the ultrasound waves, it should be noted that in the process of synthesis a sample without using ultrasonic waves, the time of magnetic stirring was equal to the time of using ultrasound waves, and the rest of the items were exactly the same as the sono-solvothermal method that shown in Fig. 1S. The powder samples that obtained were named as (BOB)-U, (BOB)$_{0.75}$(BOI)$_{0.25}$-U, (BOB)$_{0.5}$(BOI)$_{0.5}$-U, (BOB)$_{0.25}$(BOI)$_{0.75}$-U, (BOI)-U and (BOB)$_{0.75}$(BOI)$_{0.25}$ (without sonication). The schematic of the
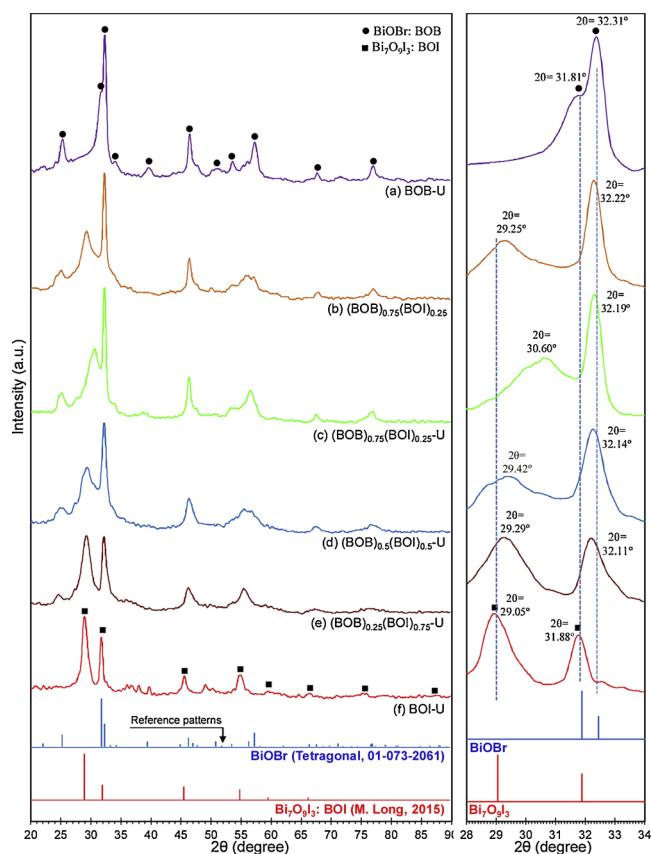
Fig. 1. XRD patterns of nanostructured $(BiOBr)_x(Bi_7O_9I_3)_{1-x}$ solid-solution nanophotocatalysts: (a) BOB-U, (b) $(BOB)_{0.75}(BOI)_{0.25}$, (c) $(BOB)_{0.75}(BOI)_{0.25}$-U, (d) $(BOB)_{0.5}(BOI)_{0.5}$-U, (e) $(BOB)_{0.25}(BOI)_{0.75}$-U and (f) BOI-U.34.

experimental setup for one-pot ultrasound-assisted solvothermal fabrication of nanostructured $(BiOBr)_x(Bi_7O_9I_3)_{1-x}$ solid-solution nanophotocatalysts is presented in Fig. 2S.

2.3. Nanophotocatalysts characterization techniques

In this study, for identifying materials and studying the crystal phase, crystal size, single crystal orientation, X-ray diffraction (XRD Siemens D5000) was used that equipped with Ca Ka in the 2θ range of 20-90° (tube operated at 30 kV and 40 mA). To determine the surface morphology and also to determine the size of the particles on the surface, the field emission scanning electron microscopy (FESEM: Mira 3-XMU Czech Republic, TESCAN) and the high resolution transmission electron microscopy equipment (HRTEM: Talos F200X, FEI, Czech) were used. Also, X-ray dot mapping (EDX dot mapping: VEGA II Detector, Czech Republic, TESCAN) employed to confirm the distribution of elements and their types in samples. Specific surface area (S_{BET}) and total cavity volume (V_c) of the nanophotocatalysts determined from the nitrogen absorption data gained from Chembet-3000 (USA, Quantachrome) and applying the Barrett–Emmett–Teller (BET) and Barrett-Joyner-Halenda (BJH) method. Identification of functional groups was attained by Fourier Transform Infrared Spectroscopy (FTIR, UNICAM 4600) in the range of 400–4000 cm^{-1} wavenumber. For calculating the band gap and evaluating the optical properties of synthesized photocatalysts the ultraviolet-visible (UV–vis) diffuse reflectance spectra (DRS) were done from 250 to 700 nm by a Scinco 4100 spectrophotometer (Shimadzu, Japan).

2.4. Experimental setup for photocatalytic performance test

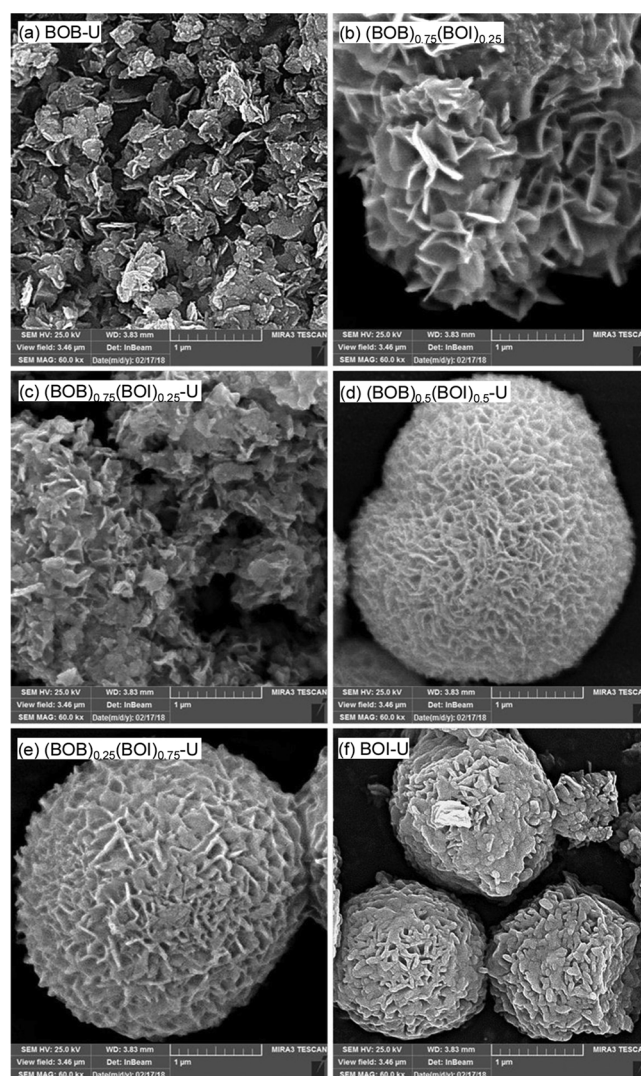In order to evaluate the photocatalytic function of the synthesized

Fig. 2. FESEM images of nanostructured $(BiOBr)_x(Bi_7O_9I_3)_{1-x}$ solid-solution nanophotocatalysts: (a) BOB-U, (b) $(BOB)_{0.75}(BOI)_{0.25}$, (c) $(BOB)_{0.75}(BOI)_{0.25}$-U, (d) $(BOB)_{0.5}(BOI)_{0.5}$-U, (e) $(BOB)_{0.25}(BOI)_{0.75}$-U and (f) BOI-U.35.

nanophotocatalysts, experiments were conducted to remove the levofloxacin (Table 1) from synthetic effluent under simulated solar light. In each experiment, 0.2 g of photocatalyst was added to 200 ml of solution containing (50 mg/L) levofloxacin. Then, in order to achieve the equilibrium of adsorption/desorption, it was placed in darkness for one hour in a Pyrex photoreactor. It was subsequently subjected to the irradiation of the 400 W halogen bulb, that manufactured by OSRAM company in Germany, which has similar characteristics to sun light. Sampling was carried out every 15 min. The photocatalyst was then separated using a centrifuge device. Subsequently, residue levofloxacin in samples was read using a Uv–vis-1800 spectrophotometer in a maximum wavelength of 287 nm. The efficiency of the removing of the pollutant by photocatalyst was calculated according to Eq. (1) that η, C_0 and C_t indicate the removal efficiency, the initial amount of pollutant after darkness and the amount of the contaminant at the time t, respectively.

$$\eta = (1 - \frac{C_t}{C_0}) \times 100 \tag{1}$$

3. Results and discussions

3.1. Nanophotocatalysts characterization

3.1.1. XRD analysis

XRD analysis is performed to identify materials and it is a technique for studying the crystal phase, crystal size, single crystal orientation, and so on. Fig. 1 illustrates the results of the XRD analysis of (BOB)-U, $(BOB)_{0.75}(BOI)_{0.25}$, $(BOB)_{0.75}(BOI)_{0.25}$-U, $(BOB)_{0.5}(BOI)_{0.5}$-U, $(BOB)_{0.25}(BOI)_{0.75}$-U, and (BOI)-U nanophotocatalysts. In the (BOB)-U sample (Fig. 1(a)), the index peaks of phase BiOBr (JCPDS NO = 01-073-2061) are observed with a cubic crystal structure at $2\theta = 25.3$, 31.8, 32.3, 46.3, 50.8, 56.4, 57.3° and in the (BOI)-U sample (Fig. 1(f)), the index peaks of phase $Bi_7O_9I_3$ correspond to the index peaks reported by Long and co-workers [43], indicating the successful synthesis of both phases. To study the structure of the solid solution that created in the photocatalysts, the XRD pattern was zoomed in the range of $2\theta = 28–34°$. As it is seen, with decreasing Br percentage, the index peak of the BiOBr at $2\theta = 32.31°$ is shifted to the left and smaller angles so this index peak for BOB-U, $(BOB)_{0.75}(BOI)_{0.25}$, $(BOB)_{0.75}(BOI)_{0.25}$-U, $(BOB)_{0.5}(BOI)_{0.5}$-U and $(BOB)_{0.25}(BOI)_{0.75}$-U nanophotocatalysts were achieved 32.31°, 32.22°, 32.19°, 32.14° and 32.11° respectively. Also, with decreasing I percentage, the index peak of the $Bi_7O_9I_3$ at $2\theta = 29.05°$ is shifted to the right and bigger angles so this index peak for (BOI)-U, $(BOB)_{0.25}(BOI)_{0.75}$-U, $(BOB)_{0.5}(BOI)_{0.5}$-U, $(BOB)_{0.75}(BOI)_{0.25}$-U and $(BOB)_{0.75}(BOI)_{0.25}$ nanophotocatalysts were achieved 29.05°, 29.29°, 29.42°, 30.06° and 29.25° respectively.

This event indicates that the separate phases of BiOBr and $Bi_7O_9I_3$ have been removed and the $(BiOBr)_x(Bi_7O_9I_3)_{1-x}$ (with or without so-nication) solid solutions structure are synthesized. In addition, the use of ultrasonic waves reduces the crystallinity of crystalline phases. Ultrasonic waves seem that lead to wide distribution of particles and an increase in the nucleation, and as a result of this cause a large number of small-sized nuclei and decreases the degree of the crystallinity of the photocatalyst.

3.1.2. FESEM analysis

Fig. 2 shows the FESEM analysis of the synthesized samples. This analysis is used to determine the surface morphology and also to determine the size of the particles on the surface. As shown in Fig. 2(a), the BOB-U (pure BiOBr) photocatalyst has the sheet morphology with the thickness in the nano range. These nanosheets are collected together and formed clusters. By creating the $(BiOBr)_x(Bi_7O_9I_3)_{1-x}$ solid solution structure, the clusters that made up from nanoparticles, are enlarged and by decreasing the amount of the x, the ball flower-like surface morphology appears. By further decreasing the amount of x, the size and volume of the ball flowers dropped and the petals become paste. So, in the $Bi_7O_9I_3$ sample (Fig. 2(f)), these dough sheets are completely dense and the spacing between them is reduced. Therefore the absorption of light reduces and the photocatalyst activity reduces. Also, by comparing Figs. 2(b) and 4 (c), it can be concluded that the use of ultrasonic waves reduces the size of the sheets and cause the uniform distribution of the particles that increases the surface area, increases active sites for light absorption and also contaminant molecules becomes more available thus photocatalytic activity increases. In Fig. 3, the surface structure of the $(BiOBr)_x(Bi_7O_9I_3)_{1-x}$ nanostructure solid solution photocatalysts is presented. In general terms, it can be stated that the synthesis of all samples was done in nanometer scale, which indicates the ability of the sono-solvothermal method to synthesize nanopowders. For example, for a $(BOB)_{0.75}(BOI)_{0.25}$-U photocatalyst, the thickness of the sheets is about 27.6 nm.

3.1.3. HRTEM analysis

To more investigate and study the detailed morphology and to confirm the crystalline phases detected by XRD analysis using the characteristic lattice fringes, HRTEM analysis was performed on the
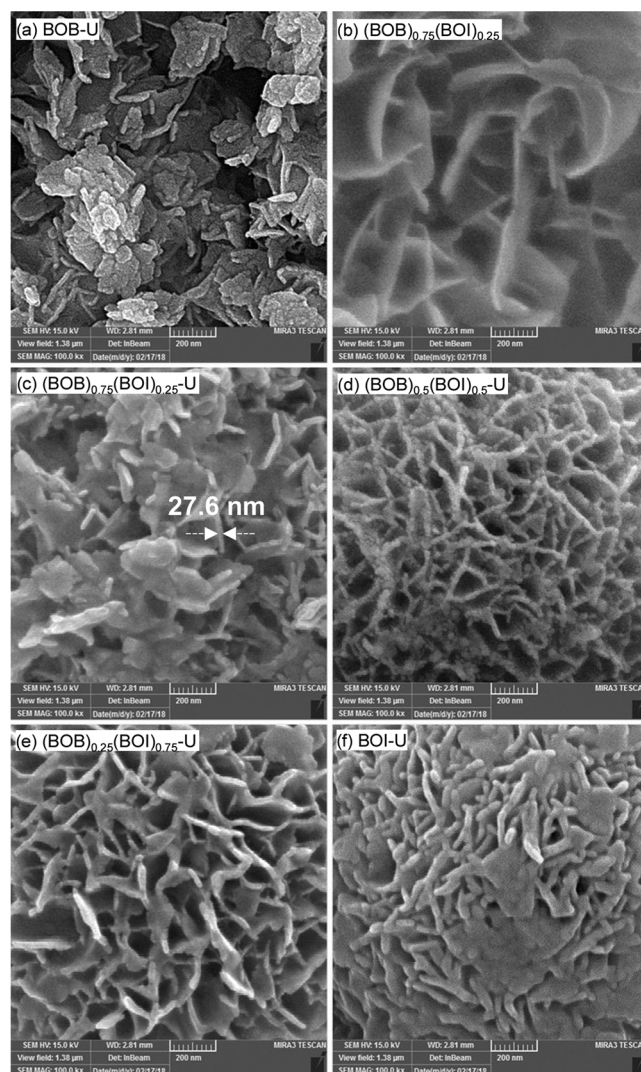

Fig. 3. Surface structure of nanostructured $(BiOBr)_x(Bi_7O_9I_3)_{1-x}$ solid-solution nanophotocatalysts: (a) $(BOB)_{0.75}(BOI)_{0.25}$ and (b) $(BOB)_{0.75}(BOI)_{0.25}$-U.36.

$(BiOBr)_{0.75}(Bi_7O_9I_3)_{0.25}$-U nanophotocatalyst as the best sample. Images obtained are demonstrated in Fig. 4. This figure displays the formation of the nanostructure in the nanophotocatalyst structure during the sono-solvothermal route. Moreover, the lattice fringes with d spacing at about 0.81 nm that may be indexed as (001) plane show the BiOBr crystalline phase and in agreement with XRD results

3.1.4. EDX analysis

The results of EDX and dot mapping analysis of (BOB)-U, $(BOB)_{0.75}(BOI)_{0.25}$, $(BOB)_{0.75}(BOI)_{0.25}$-U, and (BOI)-U are presented in Fig. 5. According to the results the presence of Br, Bi, O and I elements has been confirmed in the mentioned samples. Moreover, the distribution of elements in the samples is quite evident with respect to the dot mapping images. As it is shown in the Fig. 5, all elements are completely homogeneous and evenly distributed over the catalyst surface of (BOB)-U, $(BOB)_{0.75}(BOI)_{0.25}$-U, and (BOI)-U. It should be noted that, by comparing the sample $(BOB)_{0.75}(BOI)_{0.25}$-U and $(BOB)_{0.75}(BOI)_{0.25}$, the effect of ultrasound is also significant. As clearly seen in Fig. 5, the elements are more uniformly distributed and dispersed in the ultrasound sample.

3.1.5. BET-BJH analysis

Due to the direct effect of specific surface area and photocatalyst adsorption/desorption rate on the performance of photocatalytic
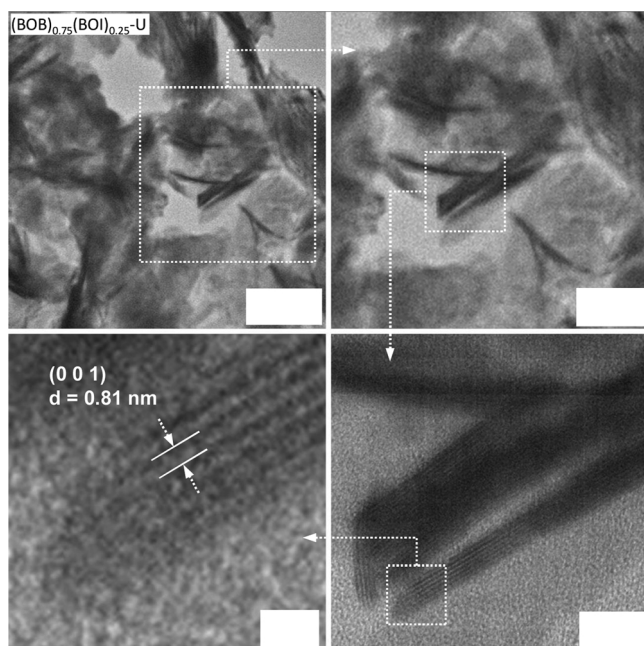
Fig. 4. HRTEM images of nanostructured $(BiOBr)_x(Bi_7O_9I_3)_{1-x}$ solid-solution photocatalyst: $(BOB)_{0.75}(BOI)_{0.25}$.37.

reactions, the use of BET-BJH analysis has a significant role in analysing the results of photocatalytic processes. The results of the photocatalytic adsorption/desorption isotherm of the BOB-U, $(BOB)_{0.75}(BOI)_{0.25}$, $(BOB)_{0.75}(BOI)_{0.25}$-U and BOI-U are depicted in Fig. 6 and the values of the specific surface area (S_{BET}), the cavity volume (V_c) and the average

diameter of the cavities (D_c) are represented in Table 2. As it is seen, the adsorption isotherm of these nanophotocatalysts is the type IV according to IUPAC classification with the hysteresis cycle, which indicates the mesoporous structure. In addition, according to the pore size distribution diagram, the pore size distribution range of the all samples which was determined by using the BJH method and the desorption branch of isotherms, was between 2 nm to the 30 nm, indicating that they have mesoporous structure. These pores can facilitate the penetration of the contaminating molecules and products, as well as have an effective role in adsorbing contaminating molecules. Also, the presence of mesoporous structure increases the light absorption, which will eventually produce more electron-hole pairs, thus improving photocatalytic activity. Moreover, the surface area for BOB-U, $(BOB)_{0.75}(BOI)_{0.25}$, $(BOB)_{0.75}(BOI)_{0.25}$-U and BOI-U samples were achieved 98.4, 114.5, 125.3 and 64.9 m^2/g respectively. As observed, the use of a solid solution structure would increase the specific surface area corresponding to the increasing the numbers of the active sites. As expected, the surface area of the $(BOB)_{0.75}(BOI)_{0.25}$-U increased after the use of ultrasonic waves in synthesis, compared to $(BOB)_{0.75}(BOI)_{0.25}$ sample. This can be attributed to the reduction in the size of the clusters and nanosheets along with increasing the number of them by using ultrasonic waves. In addition, the BOB-U sample has a higher specific area than the BOI-U. This is in line with the FESEM analysis. The cause of this event can be attributed to the densification and agglomeration of nanosheets in the BOI-U sample. Regarding the above, it seems that the $(BOB)_{0.75}(BOI)_{0.25}$-U nanophotocatalyst has a high photocatalytic function in the degradation of levofloxacin due to its high specific surface and presence of mesoporous structure.

3.1.6. FTIR analysis

FTIR analysis is one of the most common techniques for identifying and measuring molecular species, especially organic molecular species,
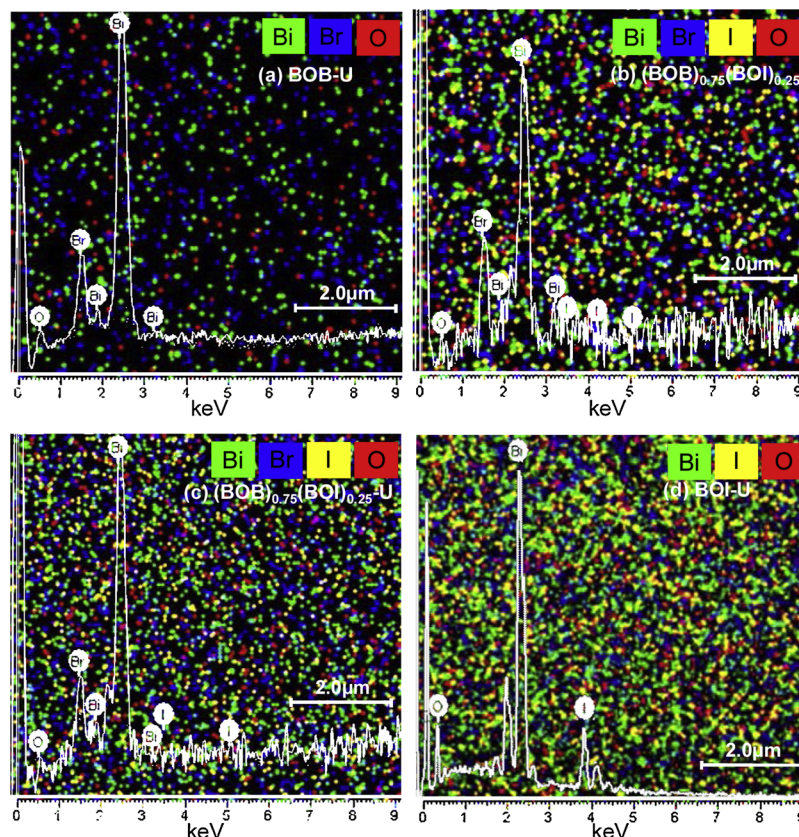

Fig. 5. EDX analysis of nanostructured $(BiOBr)_x(Bi_7O_9I_3)_{1-x}$ solid-solution nanophotocatalysts: (a) BOB-U, (b) $(BOB)_{0.75}(BOI)_{0.25}$, (c) $(BOB)_{0.75}(BOI)_{0.25}$-U, (d) $(BOB)_{0.5}(BOI)_{0.5}$-U, (e) $(BOB)_{0.25}(BOI)_{0.75}$-U and (f) BOI-U.38.
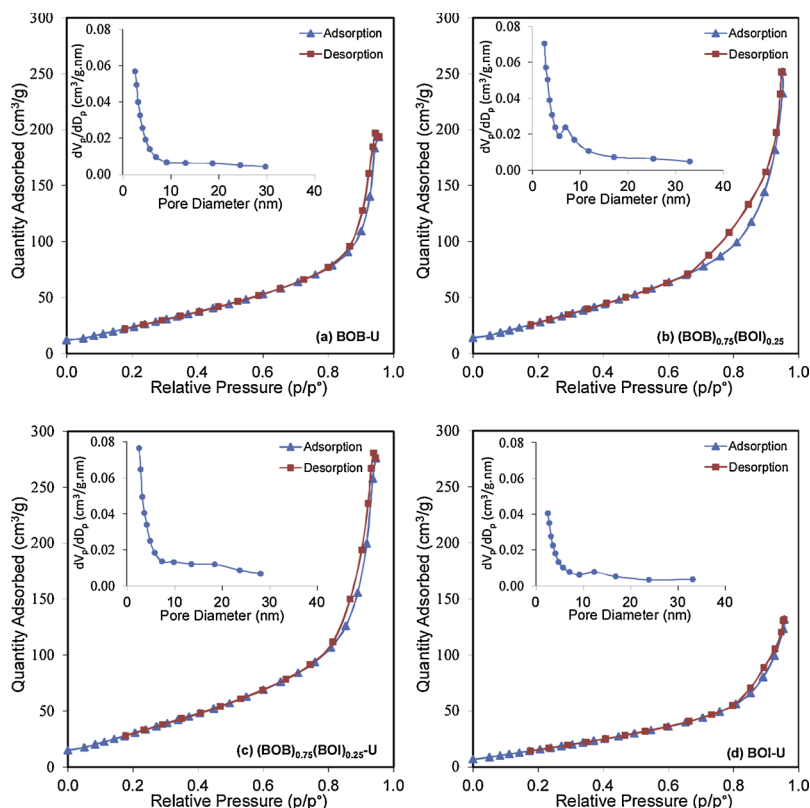
Fig. 6. Adsorption/Desorption isotherms and pore size distribution of nanostructured $(BiOBr)_x(Bi_7O_9I_3)_{1-x}$ solid-solution nanophotocatalysts: (a) BOB-U, (b) $(BOB)_{0.75}(BOI)_{0.25}$, (c) $(BOB)_{0.75}(BOI)_{0.25}$-U, (d) $(BOB)_{0.5}(BOI)_{0.5}$-U, (e) $(BOB)_{0.25}(BOI)_{0.75}$-U and (f) BOI-U.39.

Table 2
Structural properties of nanostructured $(BiOBr)_x(Bi_7O_9I_3)_{1-x}$ solid-solution nanophotocatalysts.

Nanocatalyst	Composition (wt.%)		Ultrasound Irradiation	S_{BET} (m²/g)	V_c (cm³/g)	D_c (nm)	Band Gap (eV)
	BOB: BiOBr	BOI: $Bi_7O_9I_3$					
BOB-U	100	0	Yes	98.4	0.406	11.6	2.99
$(BOB)_{0.75}(BOI)_{0.25}$	75	25	No	114.5	0.530	12.0	2.65
$(BOB)_{0.75}(BOI)_{0.25}$-U	75	25	Yes	125.3	0.589	11.4	2.43
$(BOB)_{0.5}(BOI)_{0.5}$-U	50	50	Yes	–	–	–	–
$(BOB)_{0.25}(BOI)_{0.75}$-U	25	75	Yes	–	–	–	–
BOI-U	0	100	Yes	64.9	0.275	12.1	2.52

by using its functional groups. The basis of this analysis is the ability of various molecular vibrations originating from the absorption of energy in the infrared spectral range for vibrational transmissions. Fig. 7 shows the FTIR spectra of BOB-U, $(BOB)_{0.75}(BOI)_{0.25}$, $(BOB)_{0.75}(BOI)_{0.25}$-U and BOI-U nanophotocatalysts. Peaks of 1640, 3440, 3750, and 3850 cm⁻¹ can be assigned to water molecules and hydroxyl groups [44,45]. The presence of sharp peaks at 2920 cm⁻¹ and 1050 cm⁻¹ can be attributed to the vibrational state of C–H and the tensile state of C=O [46]. Also, the adsorption numbers shown in low frequencies (below 1000 cm⁻¹) belong to the vibrational state of the Bi–O bonds [47]. Moreover, the peak that appearing at the frequency of 1390 cm⁻¹ shows the existence of Bi-Br bonds [48] and, as it is seen, this peak does not appear in the BOI-U sample (Fig. 7(c)). As it is seen, the results that obtained from FTIR analysis are in accordance with XRD and EDX analyses.

3.1.7. DRS analysis

In the DRS analysis, the absorption of the electromagnetic radiation cause the electrons on the valence layer of atoms and molecules be excited. This analysis is used for calculating the band gap and evaluating the optical properties of synthesized photocatalysts and plays an

important role on the photocatalytic activity. In Fig. 8, the DRS spectra of BOB-U, $(BOB)_{0.75}(BOI)_{0.25}$, $(BOB)_{0.75}(BOI)_{0.25}$-U and BOI-U samples are illustrated in the range of 250 nm to 700 nm. According to the absorption graph (Fig. 8(a)), it can be stated that all of the samples are active in the visible light region, but the maximum absorption edge for the $(BOB)_{0.75}(BOI)_{0.25}$-U photocatalyst is at a wavelength of about 510 nm, which in comparison with other samples, covers a wide range of wavelength for activation. Since it can generate the electron-hole pairs through the light absorption in the wavelengths lower than 510 nm (λ < 510 nm). Additionally, band gap of samples were calculated using DRS data and Kubelka-Munk equation ($αhν = A(hν − E_g)^{n/2}$). In this equation, α, h, ν, A and E_g are absorption coefficients, Planck constant, constant numbers and band gap, respectively [49]. The value of n depends on direct transmission of electrons (n = 1) and indirect transmission of electrons (n = 4) [5]. For all of the synthesized nanophotocatalysts, the value of n is 4. According to the above content, the band gaps of the samples were estimated considering with diagram Fig. 8(b) by drawing and extrapolation $(αhν)^{1/2}$ according to hν. The amount of band gap for BOB-U, $(BOB)_{0.75}(BOI)_{0.25}$, $(BOB)_{0.75}(BOI)_{0.25}$-U and BOI-U samples were obtained 2.99, 2.65, 2.43 and 2.55 eV respectively. The results show that the structure of BiOBr
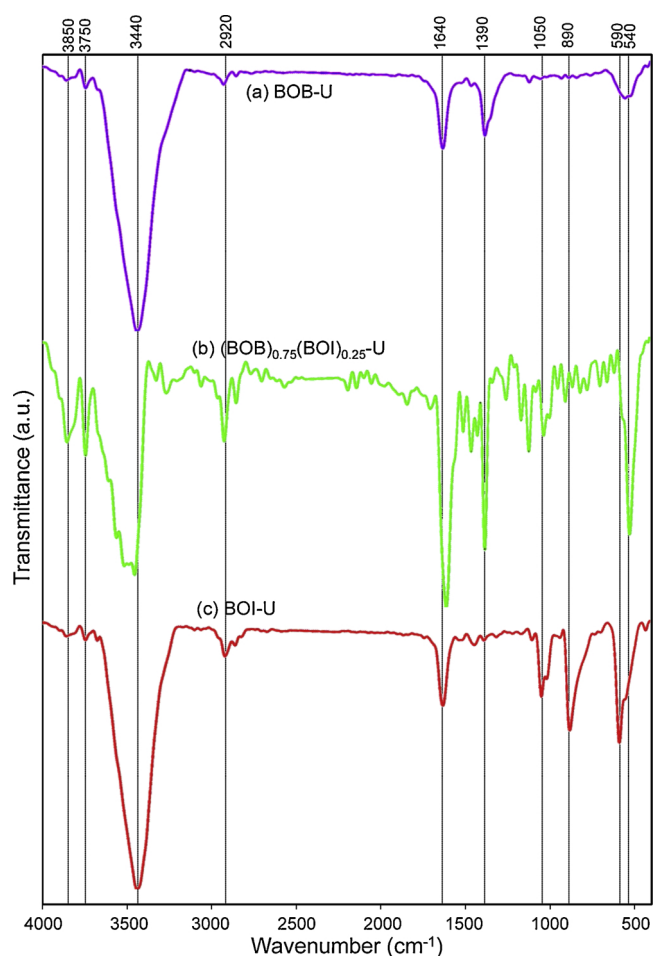
Fig. 7. FTIR analysis of nanostructured $(BiOBr)_x(Bi_7O_9I_3)_{1-x}$ solid-solution nanophotocatalysts: (a) BOB-U, (b) $(BOB)_{0.75}(BOI)_{0.25}$-U and (f) BOI-U.40.

Fig. 8. (a) UV–vis diffuse reflectance spectra and (b) plot of $(\alpha h\upsilon)^{1/2}$ versus photon energy (hυ) for nanostructured $(BiOBr)_x(Bi_7O_9I_3)_{1-x}$ solid-solution nanophotocatalysts: BOB-U, $(BOB)_{0.75}(BOI)_{0.25}$, $(BOB)_{0.75}(BOI)_{0.25}$-U and BOI-U.41.

and $Bi_7O_9I_3$ has been changed due to the formation of solid solution, leading to the emergence of a new structure with improved optical properties. In addition, the structure of the $(BOB)_{0.75}(BOI)_{0.25}$-U solid solution, that synthesized by ultrasonic waves, provides the possibility of use of low energy photons owning to an appropriate band gap, that could increase the efficiency of the photocatalytic degradation of levofloxacin from aqueous solution.

3.1.8. pH_pzc analysis

pH at the point of zero charge (pH_pzc) is one of the properties of solid materials and it is an important parameter for determining the surface charge of catalysts/adsorbents at different pH and directly affects the adsorption of pollutants and photocatalytic activity. The pH_pzc for the elected photocatalyst $((BiOBr)_{0.75}(Bi_7O_9I_3)_{0.25}$-U) is 5.7. As shown in Fig. 9, in this case, the surface charge of nanophotocatalyst is positive value at less than 5.7 and in more amounts of 5.7, it is negative. These upshots must be considered in the analysing of results that obtained in the section related to the evaluation of pH effect.

3.2. Photocatalytic degradation of antibiotic levofloxacin

3.2.1. Influence of solid-solution composition and ultrasound irradiation

In order to evaluate the photocatalytic function of the fabricated nanophotocatalysts, experiments were conducted to remove the levofloxacin from synthetic effluent under simulated sunlight. In these experiments the initial levofloxacin concentration, catalyst loading and initial pH were 50 mg/L, 1 g/L and 6, respectively.

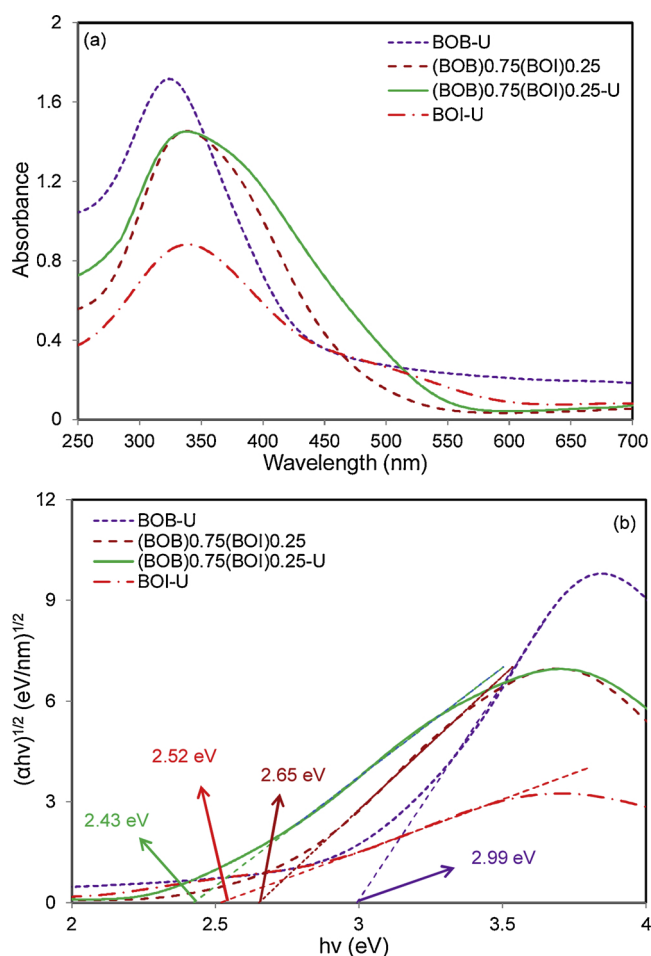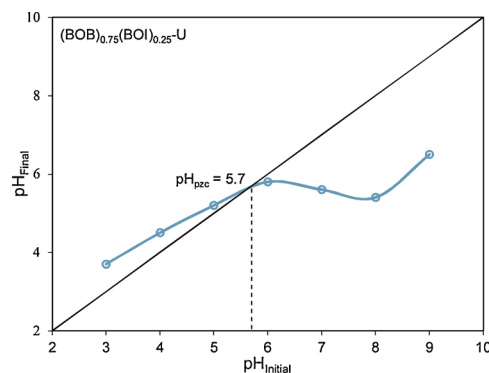According to the Fig. 10(a), the highest adsorption capacity of

Fig. 9. pH_pzc of nanostructured $(BiOBr)_x(Bi_7O_9I_3)_{1-x}$ solid-solution nanophotocatalyst: $(BOB)_{0.75}(BOI)_{0.25}$-U.42.

levofloxacin in the darkness is for $(BOB)_{0.75}(BOI)_{0.25}$-U solid solution nanophotocatalyst and the lowest adsorption capacity is for BOI-U solid solution nanophotocatalyst. This result is expected because, according to the results of the BET analysis, the $(BOB)_{0.75}(BOI)_{0.25}$-U solid solution nanophotocatalyst has the highest specific surface area. It is worth nothing that by changing the ratio of the x, the specific surface area and subsequently the amount of adsorption of the pollutant changes. According to Fig. 10(b), the percentage of pollutant degradation by BOB-U, $(BOB)_{0.75}(BOI)_{0.25}$, $(BOB)_{0.75}(BOI)_{0.25}$-U, $(BOB)_{0.5}(BOI)_{0.5}$-U,
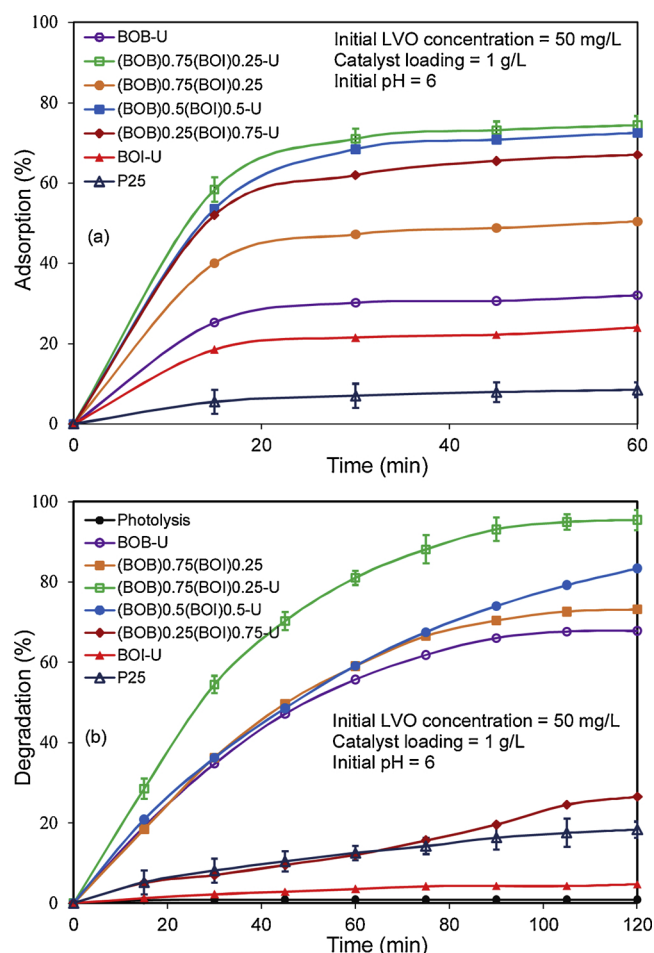
Fig. 10. Influence of nanostructured $(BiOBr)_x(Bi_7O_9I_3)_{1-x}$ solid-solution composition and ultrasound irradiation on (a) adsorption and (b) sun-light photocatalytic degradation of antibiotic levofloxacin.43.

$(BOB)_{0.25}(BOI)_{0.75}$-U and BOI-U were 67.8%`, 73.1%, 95.4%, 83.3%, 26.5%, and 4.7%, respectively. As seen, the highest activity for levofloxacin antibiotic degradation over 120 min was observed for $(BOB)_{0.75}(BOI)_{0.25}$-U solid solution nanophotocatalyst. According to various analyses, the superiority of this photocatalyst was approved. The solid solution structure of this photocatalyst increases the amount of adsorbing contaminants. Additionally, due to the adequate band gap energy, it improves the ability to absorb light at the wide region of visible light. It is also possible that the rate of recombination of charge carriers is reduced compared with the pure state of each nanophotocatalyst. Moreover, using the ultrasonic waves in producing this photocatalyst causes the uniform and proper distribution of particles and provides more surface of photocatalyst to be available for the pollutant molecules. Furthermore, in order to compare the photocatalytic performance of the TiO_2 (P25) and ball-flowerlike mesoporous $(BiOBr)_{0.75}(Bi_7O_9I_3)_{0.25}$-U nanophotocatalyst in the levofloxacin degradation, a reactor test was performed on commercial Degussa P25 in the same conditions. As shown in Fig. 10, the photocatalytic degradation rate of levofloxacin was obtained 18.3%, whiles the degradation efficiency of this antibiotic after 120 min irradiation was 95.4% over the $(BiOBr)_{0.75}(Bi_7O_9I_3)_{0.25}$-U nanophotocatalyst, indicating the excellent performance of this solid solution nanophotocatalyst.

Table 3 shows levofloxacin degradation efficiencies with different photocatalysts in research papers that reported in last five years. As seen in this table, the mentioned photocatalysts has eliminated very little concentration of levofloxacin contaminant (5 or 10 mg/L), even when mixed with precious metals such as silver and gold. So it can be

stated that due to the cost-effectiveness, the high percentage of degradation for high concentration of levofloxacin antibiotic (50 mg/L) and also the low irradiation time, nanophotocatalyst of this study that synthesized with ultrasonic waves is best in its kind. Therefore, ball-flowerlike mesoporous $(BiOBr)_{0.75}(Bi_7O_9I_3)_{0.25}$-U nanophotocatalyst has prominent photocatalytic activity and wide application for degrading antibiotics.

3.2.2. Influence of pH

The initial pH of the solution affect the photocatalyst surface electrical charge, hence it can play an important role in the adsorption and subsequently degradation of contaminants. Fig. 11 shows the effect of pH on the degradation of the levofloxacin antibiotic over the $(BiOBr)_{0.75}(Bi_7O_9I_3)_{0.25}$-U nanostructured photocatalyst. In this experiment the initial levofloxacin concentration was 50 mg/L, catalyst loading was 1 g/L and influence of three different pH (pH = 2, 6 and 11) was evaluated.

As seen in this Figure, the removal percentage at pH = 2, 6, and 11 obtained 51.9, 95.4 and 7.5%, respectively. According to the obtained number for pH_{pzc}, which is about 5.7, the surface charge of the photocatalyst at this pH is the zwitterion (the equality of the number of positive and negative charges on the surface), and at higher or lower values of this pH the surface is negative and positive, respectively. Besides, levofloxacin antibiotic has two pK_a values, that pK_{a1} and pK_{a2} are 5.33 and 8.07, respectively [50]. Therefore, at the pH = 2, levofloxacin will be a cationic molecule and surface charge of photocatalyst will also be positive, so, the existing electrostatic repulsion force reduces the adsorption and subsequently the percentage of degradation decreases. Furthermore, there is a limitation in the surface adsorption at the pH = 11due to the repulsive force between the anionic levofloxacin and the negative surface charge of the photocatalyst. However, as it is seen, at the pH = 2, the resulting efficiency is greater than pH = 11. This event could be interpreted as follows: at the pH = 2, the excited electrons that reach to the surface of photocatalyst can be consumed by parts of the surface that have the partial positive charge or by the existing H^+ within the solution. In this case, the amount of recombination of electron-hole pairs on the surface will greatly be reduced, and further holes can be consumed in the pathway of degradation of levofloxacin. In contrast, at pH = 11 the holes, that reach the surface of the photocatalyst, are used by the parts of the surface that have the partial negative charge or by the existing OH^- within the solution, while the hole is a main reactive species in the levofloxacin photodegradation. At pH = 6, the surface charge of the photocatalyst and the ionization condition of levofloxacin could be reversible between positive and neutral state, so the presence of cavities is greater than pH = 11 and the result of degradation efficiency is expected.

3.2.3. Influence of photocatalyst loading

Fig. 12 shows the effect of the photocatalyst loading on the degradation of the levofloxacin antibiotic. In this experiment the initial levofloxacin concentration was 50 mg/L, initial pH was 6 and in order to determine the optimum loading amount, 0.5, 1 and 1.5 g/L of elected photocatalyst $((BiOBr)_{0.75}(Bi_7O_9I_3)_{0.25}$-U) was considered. The percentage of degradation for these loads was 30.2%, 95.4% and 72.8%, respectively. These results can be explained as follows: by increasing the loading value from 0.5 to 1 g/L, the numbers of available active sites to degrade pollutants have increased, so the removal efficiency has increased. However, with increasing loading from 1 to 1.5 g/L, the efficiency of the levofloxacin degradation decreases due to the increasing of opacity, light scattering, and presumably decreasing in the number of active sites (owing to the fumigation and accumulation of photocatalyst particles). Therefore, optimal loading for photocatalyst was obtained 1 g/L.
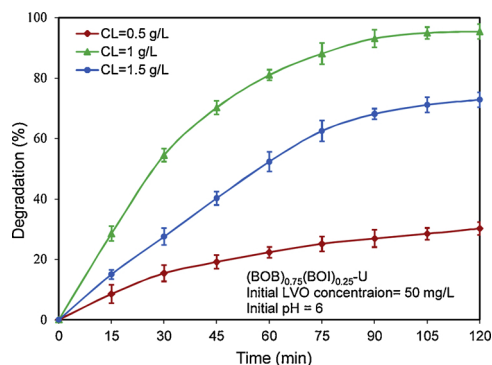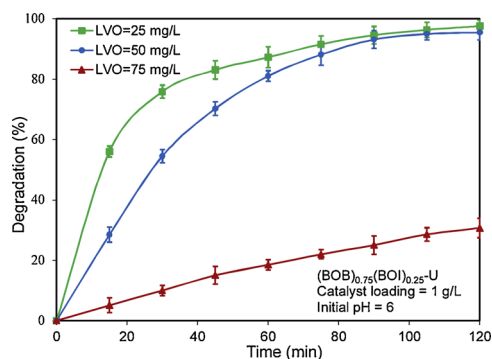
3.2.4. Effect of antibiotic levofloxacin concentration

Another effective parameter on the photocatalytic process efficiency

Table 3
Comparison of antibiotic LVO photodegradation with various nanophotocatalysts.

| Photocatalysts	Reaction Conditions	Degradation %	Reference
$(BiOBr)_x(Bi_7O_9I_3)_{1-x}$	50 mg/L, 120 min, Solar light	95.4%	this study
Ag/AgBr/BiOBr	10 mg/L, 90 min, Visible light	74%	[48]
Bi_2WO_6	10 mg/L, 140 min, Visible light	80%	[50]
Ag_2O/TiO_2	10 mg/L, 90 min, Visible light	81%	[51]
$Ag_2CO_3/CeO_2/AgBr$	10 mg/L, 40 minutes, Visible light	87.63%	[52]
$Au-Pd/TiO_2$	5 mg/L, 60 min, Visible light	95%	[53]
Reduced graphene oxide-CdS	10 mg/L, 60 min, Visible light	82.7%	[54]
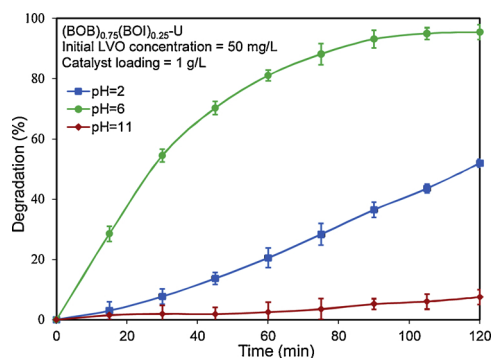
Fig. 11. Influence of pH on sun-light photocatalytic degradation of antibiotic levofloxacin over $(BOB)_{0.75}(BOI)_{0.25}$-U solid-solution nanophotocatalyst.44.

Fig. 12. Influence of catalyst loading on sun-light photocatalytic degradation of antibiotic levofloxacin over $(BOB)_{0.75}(BOI)_{0.25}$-U solid-solution nanophotocatalyst.44.

Fig. 13. Influence of pollutant concentration on sun-light photocatalytic degradation of antibiotic levofloxacin over $(BOB)_{0.75}(BOI)_{0.25}$-U solid-solution nanophotocatalyst.45.

is the initial concentration of contaminants. In this regard, the effect of the contaminant concentration on the degradation of levofloxacin antibiotic under simulated sunlight was evaluated for the $(BiOBr)_{0.75}(Bi_7O_9I_3)_{0.25}$-U nanostructure photocatalyst and results are

displayed in Fig. 13. In this experiment the catalyst loading was 1 g/L, initial pH was 6 and different initial levofloxacin concentrations (25, 50 and 75 mg/L) were evaluated. The degradation percentage of levofloxacin at the initial concentrations of 25, 50 and 75 mg/L was gained 97.9%, 95.4% and 30.7%, respectively. As it is seen, the η decreases with increasing the concentration of the antibiotic. The cause of this event can be stated as follows: with increasing concentrations of levofloxacin, the amount of pollutant that is adsorbed on the photocatalyst surface increases. This event reduces the amount of the active species, such as oxygen radical which created by surface activity of photocatalyst under light. Additionally, the amount of photons that is absorbed by the pollutant will also increase. So, fewer photons could get to the surface of the photocatalyst.

3.2.5. Reusability study

The photocatalyst stability is a determinant factor for its practical application. The stability and re-usability of $(BiOBr)_{0.75}(Bi_7O_9I_3)_{0.25}$-U nanophotocatalyst was evaluated by four cycles, that the results are shown in Fig. 14. After each cycle, the photocatalyst was separated from the solution and washed with the deionized water and then dried at 110 °C. The results show that $(BiOBr)_{0.75}(Bi_7O_9I_3)_{0.25}$-U nanophotocatalyst has a relatively good stability. It should be noted that at the end of the fourth cycle, the used photocatalyst was characterized with XRD analysis and compared with the fresh photocatalyst XRD pattern. As shown in Fig. 15, the photocatalyst structure has not changed since the use, indicating the photocatalyst chemical stability. The only change observed is the reduction in the intensity of some of the index peaks in the photocatalyst structure that could be due to the leaching of active phases. In general, the observed reduction in degradation efficiency after the fourth cycle can be attributed to the leaching of active phases and catalyst poisoning with contaminants or by-products. For accurate evaluation and evaluation the formation of Bi oxycarbonate the used photocatalyst was characterized with EDX-dot mapping analysis and compared with the fresh photocatalyst EDX-dot mapping pattern. As shown in Fig. 16, the photocatalyst structure of used sample has not changed, indicating the photocatalyst chemical stability. According to the result, the presence of Br, Bi, O and I elements has been confirmed
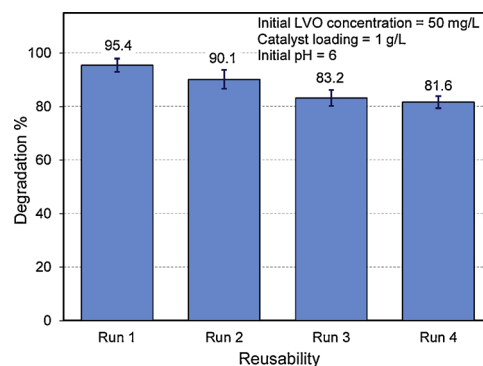
Fig. 14. Reusability of $(BOB)_{0.75}(BOI)_{0.25}$-U solid-solution nanophotocatalyst toward sun-light photocatalytic degradation of antibiotic levofloxacin.45.
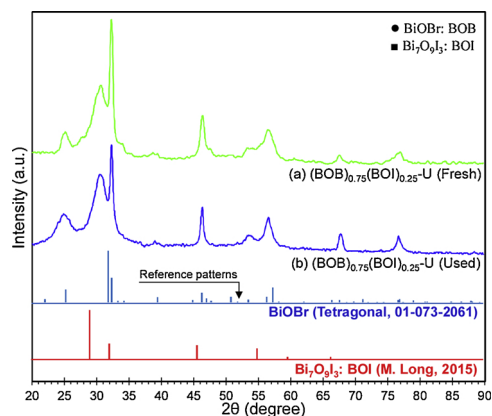
Fig. 15. XRD patterns of fresh and used $(BOB)_{0.75}(BOI)_{0.25}$-U solid-solution nanophotocatalyst: (a) Fresh catalyst and (b) Used catalyst.46.
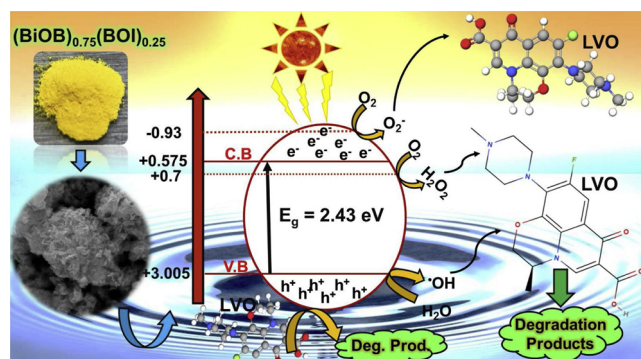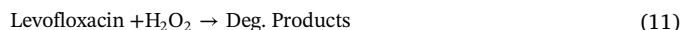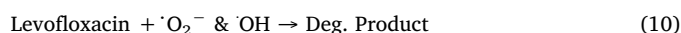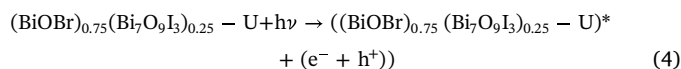

Fig. 17. Reaction mechanism for sun-light photocatalytic degradation of antibiotic levofloxacin over $(BOB)_{0.75}(BOI)_{0.25}$-U solid-solution nanophotocatalyst.47.

in this sample. Moreover, the carbon element was not seen in this analysis which was predicted by result of XRD analysis. Meaning, Bi oxycarbonate is not formed in this sample. Also, the distribution of elements in the sample is quite evident with respect to the dot mapping image.

3.3. Reaction pathway for antibiotic levofloxacin photocatalytic degradation

The proposed mechanism for the degradation of levofloxacin over $(BiOBr)_{0.75}(Bi_7O_9I_3)_{0.25}$-U nanophotocatalyst under simulated sunlight is shown in Fig. 17. E_{VB} and E_{CB} of the $(BiOBr)_{0.75}(Bi_7O_9I_3)_{0.25}$-U nanophotocatalyst was calculated by using Eqs. (2) and (3) [16] with a band gap of 2.43 eV.

$$E_{CB} = X - E_e - E_g \tag{2}$$

$$E_{VB} = E_{CB} + E_g \tag{3}$$

In the Eqs. (2) and (3) X, E_{VB}, E_{CB}, E_e and E_g are the semiconductor's absolute electronegativity, the valence band energy, the conduction band energy, the energy of free electrons on the hydrogen scale (E_e = 4.9 eV) and the band gap energy, respectively. According to the above equations, E_{CB} and E_{VB} for $(BiOBr)_{0.75}(Bi_7O_9I_3)_{0.25}$-U nanophotocatalyst were calculated about $+0.58$ and $+3$ eV, respectively. When the photocatalyst is under the sunlight and receives equal or greater energy than the band gap energy, the electrons on the semiconductor's valence layer, are transferred to their conduction layer and instead, the hole remains in the valence layer.

Also, according to the oxidation-reduction potential $O_2/\cdot O_2^- = -0.28$ eV [2], there is the possibility of producing oxygen radicals by

negative energy levels of conduction band. Moreover, due to the potential of the semiconductor's valence layer is greater than the standard potential of the $\cdot OH/OH$- ($+2.4$ eV) and $\cdot OH/H_2O$ ($+2.8$ eV), it can be expected that the holes are reacted with water and the hydroxyl ions and produce $\cdot OH$ radicals. Radicals and holes that are present in the environment could attack the contaminant molecules and lead to their destruction. According to the above, the following reactions can be proposed to remove the pollutant:

$$(BiOBr)_{0.75}(Bi_7O_9I_3)_{0.25} - U + h\nu \rightarrow ((BiOBr)_{0.75}(Bi_7O_9I_3)_{0.25} - U)^*$$
$$+ (e^- + h^+)) \tag{4}$$

$$O_2 + e^- \rightarrow \cdot O_2^- \tag{5}$$

$$O_2 + 2e^- + 2H^+ \rightarrow H_2O_2 \tag{6}$$

$$H_2O + h^+ \rightarrow \cdot OH \tag{7}$$

$$OH^- + h^+ \rightarrow \cdot OH \tag{8}$$

$$\text{Levofloxacin} + h^+ \rightarrow \text{Deg. Products} \tag{9}$$

$$\text{Levofloxacin} + \cdot O_2^- \ \& \ \cdot OH \rightarrow \text{Deg. Product} \tag{10}$$

$$\text{Levofloxacin} + H_2O_2 \rightarrow \text{Deg. Products} \tag{11}$$

3.4. Kinetic evaluation of antibiotic levofloxacin degradation reaction

According to the Langmuir-Hinshelwood Kinetic model [47], the photocatalytic elimination rate of levofloxacin is calculated by Eq. (12).
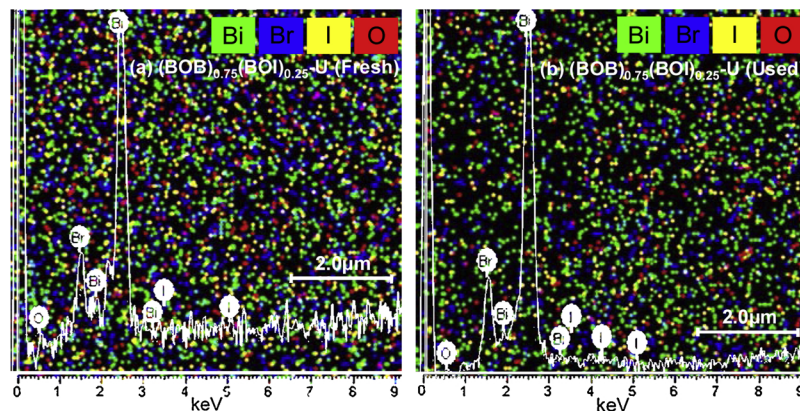
$$\ln(C/C_0) = k_{app}t \tag{12}$$

Fig. 16. EDX analysis of fresh and used $(BOB)_{0.75}(BOI)_{0.25}$-U solid-solution nanophotocatalyst: (a) Fresh catalyst and (b) Used catalyst.46.

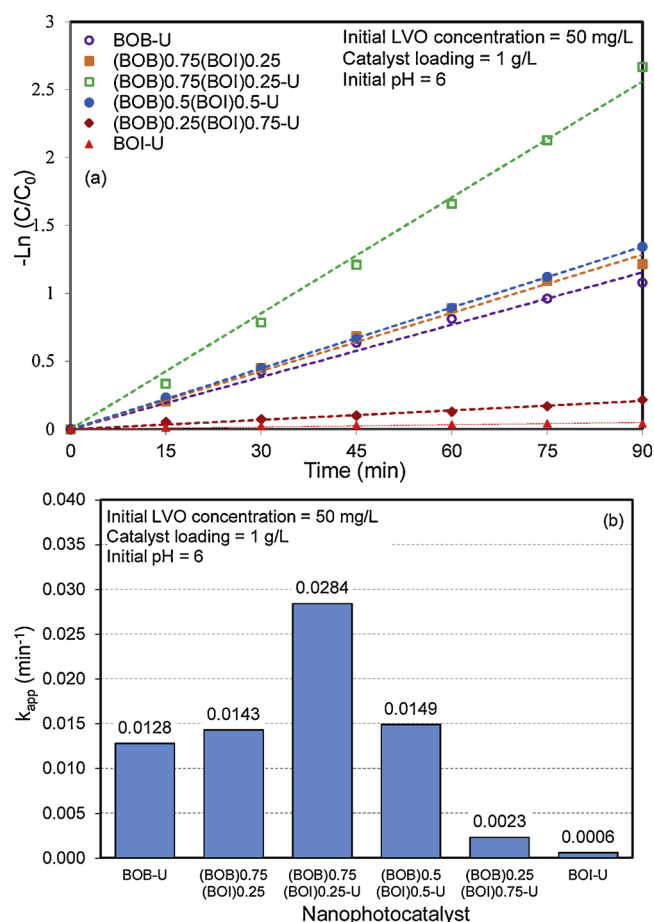**Fig. 18.** Kinetic consideration of nanostructured $(BiOBr)_x(Bi_7O_9I_3)_{1-x}$ solid-solution nanophotocatalysts toward sun-light photocatalytic degradation of antibiotic levofloxacin: (a) -ln(C/C$_0$) and (b) rate constant.48.

In this equation, C_0 is the initial concentration of levofloxacin after darkness (mg/L), C is the concentration of levofloxacin at time t (mg/L) and k_{app} is the apparent pseudo first order velocity. Regarding Fig. 18(a) and (b), the $(BiOBr)_{0.75}(Bi_7O_9I_3)_{0.25}$-U solid solution nanophotocatalyst compared to other photocatalysts has the highest apparent pseudo first order velocity (0.0284 min^{-1}) that regarding to the above explanations is expected.

4. Conclusions

The novel $(BiOBr)_x(Bi_7O_9I_3)_{1-x}$ solid solution nanophotocatalysts with different x values (x = 0, 0.25, 0.5, 0.75 and 1) were successfully synthesized with the facile one-pot sono-solvothermal method. The photocatalytic activity of the synthesized nanophotocatalysts was evaluated by the degradation of 50 mg/L levofloxacin under simulated solar light irradiation during 120 min. According to the performed evaluations, the value of the x has a great impact on the photocatalytic activity. The highest adsorption capacity of the levofloxacin in the darkness and photo-degradation of levofloxacin was gained for $(BOB)_{0.75}(BOI)_{0.25}$-U solid solution nanophotocatalyst. Because, by using the ultrasonic waves in producing this photocatalyst, distribution of particles could be uniform and so more surface of photocatalyst could be available to the pollutant and the BET-BJH analysis also confirmed this reason and showed that the $(BOB)_{0.75}(BOI)_{0.25}$-U solid solution nanophotocatalyst had the highest specific surface area and total pore volume, that facilitated the penetration of pollutant molecules. Also according to the DRS analysis, this sample could be activated in the more region of the solar spectrum in compared with other samples.

Moreover, owing to the great formation of solid solution with x = 0.75, the rate of recombination was presumably reduced compared with the pure state of each nanophotocatalyst. The results of the reusability test also showed that $(BiOBr)_{0.75}(Bi_7O_9I_3)_{0.25}$-U solid solution nanophotocatalyst had a good stability and had a good photocatalytic activity even at the end of the fourth cycle.

Appendix A. Supplementary data

Supplementary material related to this article can be found, in the online version, at doi:https://doi.org/10.1016/j.apcatb.2019.02.021.

References

[1] I. Michael, E. Hapeshi, C. Michael, D. Fatta-Kassinos, Solar Fenton and solar TiO2 catalytic treatment of ofloxacin in secondary treated effluents: evaluation of operational and kinetic parameters, Water Res. 44 (2010) 5450–5462.
[2] S. Heidari, M. Haghighi, M. Shabani, Ultrasound assisted dispersion of Bi2Sn2O7-C3N4 nanophotocatalyst over various amount of zeolite Y for enhanced solar-light photocatalytic degradation of tetracycline in aqueous solution, Ultrason. Sonochem. 43 (2018) 61–72.
[3] K.H. Hama Aziz, H. Miessner, S. Mueller, D. Kalass, D. Moeller, I. Khorshid, M.A.M. Rashid, Degradation of pharmaceutical diclofenac and ibuprofen in aqueous solution, a direct comparison of ozonation, photocatalysis, and non-thermal plasma, Chem. Eng. J. 313 (2017) 1033–1041.
[4] H. Fallahi Motlagh, M. Haghighi, M. Shabani, Sono-solvothermal fabrication of ball-flowerlike Bi2O7Sn2-Bi7O9I3 nanophotocatalyst with efficient solar-light-driven activity for degradation of antibiotic tetracycline, Sol. Energy 180 (2019) 25–38.
[5] M. Shabani, M. Haghighi, D. Kahforoushan, One-pot combustion fabrication of grain-like mesoporous intra-heterostructure BixOyClz nanophotocatalyst with substantial solar-light-driven degradation of antibiotic ofloxacin: influence of various fuels, Catal. Sci. Technol. 8 (2018) 4052–4069.
[6] Q.-Q. Zhang, G.-G. Ying, C.-G. Pan, Y.-S. Liu, J.-L. Zhao, Comprehensive evaluation of antibiotics emission and fate in the river basins of China: source analysis, multimedia modeling, and linkage to bacterial resistance, Environ. Sci. Technol. 49 (2015) 6772–6782.
[7] K.D. Brown, J. Kulis, B. Thomson, T.H. Chapman, D.B. Mawhinney, Occurrence of antibiotics in hospital, residential, and dairy effluent, municipal wastewater, and the Rio Grande in New Mexico, Sci. Total Environ. 366 (2006) 772–783.
[8] O.H. Yakubu, Pharmaceutical wastewater effluent-source of contaminants of emerging concern: phytotoxicity of metronidazole to soybean (Glycine max), Toxics 5 (2017) 10.
[9] K.M. Gani, A.A. Kazmi, Contamination of emerging contaminants in indian aquatic sources: first overview of the situation, J. Hazard. Toxic Radioact. Waste 21 (2016) 04016026.
[10] A. Shraim, A. Diab, A. Alsuhaimi, E. Niazy, M. Metwally, M. Amad, S. Sioud, A. Dawoud, Analysis of some pharmaceuticals in municipal wastewater of Almadinah Almunawarah, Arab. J. Chem. 10 (2017) S719–S729.
[11] G. Gupta, A. Kaur, A. Sinha, S.K. Kansal, Photocatalytic degradation of levofloxacin in aqueous phase using Ag/AgBr/BiOBr microplates under visible light, Mater. Res. Bull. 88 (2017) 148–155.
[12] A. Kaur, S.K. Kansal, Bi2WO6 nanocuboids: an efficient visible light active photocatalyst for the degradation of levofloxacin drug in aqueous phase, Chem. Eng. J. 302 (2016) 194–203.
[13] M. Maleki, M. Haghighi, Sono-dispersion of CuS-CdS over TiO2 in one-pot hydrothermal reactor as visible-light-driven nanostructured photocatalyst, J. Mol. Catal. A Chem. 424 (2016) 283–296.
[14] A. Ghalajkhani, M. Haghighi, M. Shabani, Efficient photocatalytic degradation of methylene blue in aqueous solution over flowerlike nanostructured MoS2-FeZnO staggered heterojunction under simulated solar-light irradiation, J. Photochem. Photobiol. A: Chem. 359 (2018) 145–156.
[15] L. Yosefi, M. Haghighi, S. Allahyari, Solvothermal synthesis of flowerlike p-BiOI/n-ZnFe2O4 with enhanced visible light driven nanophotocatalyst used in removal of acid Orange 7 from wastewater, Sep. Purif. Technol. 178 (2017) 18–28.
[16] M. Shabani, M. Haghighi, D. Kahforoushan, A. Haghighi, Mesoporous-mixed-phase of hierarchical bismuth oxychlorides nanophotocatalyst with enhanced photocatalytic application in treatment of antibiotic effluents, J. Clean. Prod. 207 (2019) 444–457.
[17] M. Zarrabi, M. Haghighi, R. Alizadeh, Sonoprecipitation dispersion of ZnO nanoparticles over graphene oxide used in photocatalytic degradation of methylene blue in aqueous solution: influence of irradiation time and power, Ultrason. Sonochem. 48 (2018) 370–382.

[18] E. Saber Khatibi, M. Haghighi, S. Mahboob, Efficient surface design of reduced graphene oxide, carbon nanotube and carbon active with cupper nanocrystals for enhanced simulated-solar-Light photocatalytic degradation of acid orange in water, Appl. Surf. Sci. 465 (2019) 937–949.

[19] K.C. Kemp, H. Seema, M. Saleh, N.H. Le, K. Mahesh, V. Chandra, K.S. Kim, Environmental applications using graphene composites: water remediation and gas adsorption, Nanoscale 5 (2013) 3149–3171.

[20] M. Moradi, M. Haghighi, S. Allahyari, Precipitation dispersion of Ag-ZnO nanocatalyst over functionalized multiwall carbon nanotube used in degradation of acid orange from wastewater, Process. Saf. Environ. Prot. 107 (2017) 414–427.

[21] M.S. Ghodrati, M. Haghighi, J.S. Soltan Mohammadzadeh, B. Pourabas, E. Pipelzadeh, Phenol decomposition under sunlight using a sonochemically synthesized CdSe/TiO2 nanocatalyst, React. Kinet. Mech. Catal. 104 (2011) 49–60.

[22] S.-Y. Lee, S.-J. Park, TiO₂ photocatalyst for water treatment applications, J. Ind. Eng. Chem. 19 (2013) 1761–1769.

[23] S. Prabhu, L. Cindrella, O.J. Kwon, K. Mohanraju, Superhydrophilic and self-cleaning rGO-TiO₂ composite coatings for indoor and outdoor photovoltaic applications, Sol. Energy Mater. Sol. Cells 169 (2017) 304–312.

[24] S. Barthwal, N.B. Singh, ZnO-CNT nanocomposite: a device as electrochemical sensor, Mater. Today: Proc. 4 (2017) 5552–5560.

[25] S. Dong, Y. Li, J. Sun, C. Yu, Y. Li, J. Sun, Facile synthesis of novel ZnO/RGO hybrid nanocomposites with enhanced catalytic performance for visible-light-driven photodegradation of metronidazole, Mater. Chem. Phys. 145 (2014) 357–365.

[26] M.N. Chong, B. Jin, C.W. Chow, C. Saint, Recent developments in photocatalytic water treatment technology: a review, Water Res. 44 (2010) 2997–3027.

[27] B. Weng, F. Xu, J. Xu, Hierarchical structures constructed by BiOX (X = Cl, I) nanosheets on CNTs/carbon composite fibers for improved photocatalytic degradation of methyl orange, J. Nanoparticle Res. 16 (2014) 2766.

[28] A.C. Mera, H. Váldes, F.J. Jamett, M. Meléndrez, BiOBr microspheres for photocatalytic degradation of an anionic dye, Solid State Sci. 65 (2017) 15–21.

[29] X. Meng, Z. Zhang, Bismuth-based photocatalytic semiconductors: introduction, challenges and possible approaches, J. Mol. Catal. A Chem. 423 (2016) 533–549.

[30] D.S. Bhachu, S.J. Moniz, S. Sathasivam, D.O. Scanlon, A. Walsh, S.M. Bawaked, M. Mokhtar, A.Y. Obaid, I.P. Parkin, J. Tang, Bismuth oxyhalides: synthesis, structure and photoelectrochemical activity, Chem. Sci. 7 (2016) 4832–4841.

[31] A. Di Paola, E. García-López, G. Marcì, L. Palmisano, A survey of photocatalytic materials for environmental remediation, J. Hazard. Mater. 211 (2012) 3–29.

[32] M. Shang, W. Wang, L. Zhang, Preparation of BiOBr lamellar structure with high photocatalytic activity by CTAB as Br source and template, J. Hazard. Mater. 167 (2009) 803–809.

[33] F.-t. Li, Q. Wang, X.-j. Wang, B. Li, Y.-j. Hao, R.-h. Liu, D.-s. Zhao, In-situ one-step synthesis of novel BiOCl/Bi₂₄O₃₁Cl₁₀ heterojunctions via self-combustion of ionic liquid with enhanced visible-light photocatalytic activities, Appl. Catal. B: Environ. 150 (2014) 574–584.

[34] M. Gao, D. Zhang, H. Li, X. Pu, X. Shao, W. Li, Enhanced photocatalytic activity of AgCl/BiOCl heterostructures synthesized by a one-pot combustion method, Mater. Lett. 159 (2015) 406–409.

[35] F. Perreault, A.F. De Faria, M. Elimelech, Environmental applications of graphene-based nanomaterials, Chem. Soc. Rev. 44 (2015) 5861–5896.

[36] T. Wu, X. Li, D. Zhang, F. Dong, S. Chen, Efficient visible light photocatalytic oxidation of NO with hierarchical nanostructured 3D flower-like BiOClₓBr₁₋ₓ solid solutions, J. Alloys. Compd. 671 (2016) 318–327.

[37] Y. Na, Y.-I. Kim, D. Won Cho, D. Pradhan, Y. Sohn, Adsorption/photocatalytic performances of hierarchical flowerlike BiOBrₓCl₁₋ₓ nanostructures for methyl orange, Rhodamine B and methylene blue, Mater. Sci. Semicond. Process. 27 (2014) 181–190.

[38] Z. Jia, F. Wang, F. Xin, B. Zhang, Simple solvothermal routes to synthesize 3D biOBrₓI₁₋ₓ microspheres and their visible-light-induced photocatalytic properties, Ind. Eng. Chem. Res. 50 (2011) 6688–6694.

[39] H. Lin, X. Li, J. Cao, S. Chen, Y. Chen, Novel I−doped BiOBr composites: modulated valence bands and largely enhanced visible light phtotocatalytic activities, Catal. Commun. 49 (2014) 87–91.

[40] H. Huang, X. Han, X. Li, S. Wang, P.K. Chu, Y. Zhang, Fabrication of multiple heterojunctions with tunable visible-light-active photocatalytic reactivity in BiOBr–BiOI full-range composites based on microstructure modulation and band structures, ACS Appl. Mater. Interfaces 7 (2015) 482–492.

[41] H. Cheng, B. Huang, Y. Dai, Engineering BiOX (X = Cl, Br, I) nanostructures for highly efficient photocatalytic applications, Nanoscale 6 (2014) 2009–2026.

[42] Y. Huo, J. Zhang, M. Miao, Y. Jin, Solvothermal synthesis of flower-like BiOBr microspheres with highly visible-light photocatalytic performances, Appl. Catal. B: Environ. 111 (2012) 334–341.

[43] M. Long, P. Hu, H. Wu, Y. Chen, B. Tan, W. Cai, Understanding the composition and electronic structure dependent photocatalytic performance of bismuth oxyiodides, J. Mater. Chem. A 3 (2015) 5592–5598.

[44] O. Mehraj, B.M. Pirzada, N.A. Mir, M.Z. Khan, S. Sabir, A highly efficient visible-light-driven novel p-n junction Fe₂O₃/BiOI photocatalyst: Surface decoration of BiOI nanosheets with Fe2O3 nanoparticles, Appl. Surf. Sci. 387 (2016) 642–651.

[45] S. Wu, J. Fang, X. Hong, K.S. Hui, Y. Chen, Facile preparation and characterization of BiOI–rectorite composite with high adsorptive capacity and photocatalytic activity, Dalton Trans. 43 (2014) 2611–2619.

[46] Z. Liu, W. Xu, J. Fang, X. Xu, S. Wu, X. Zhu, Z. Chen, Decoration of BiOI quantum size nanoparticles with reduced graphene oxide in enhanced visible-light-driven photocatalytic studies, Appl. Surf. Sci. 259 (2012) 441–447.

[47] H. Liu, W.-R. Cao, Y. Su, Z. Chen, Y. Wang, Bismuth oxyiodide–graphene nanocomposites with high visible light photocatalytic activity, J. Colloid Interface Sci. 398 (2013) 161–167.

[48] Y. Li, Z. Song, Z. Yin, Q. Kuang, R. Wan, Y. Zhou, Q. Liu, J. Qiu, Z. Yang, Investigation on the upconversion emission in 2D BiOBr:Yb³⁺/Ho³⁺ nanosheets, Spectrochim. Acta A. Mol. Biomol. Spectrosc. 150 (2015) 135–141.

[49] L. Yosefi, M. Haghighi, Fabrication of nanostructured flowerlike p-BiOI/p-NiO heterostructure and its efficient photocatalytic performance in water treatment under visible-light irradiation, Appl. Catal. B: Environ. 220 (2018) 367–378.

[50] M.O. Koeppe, R. Cristofoletti, E.F. Fernandes, S. Storpirtis, H.E. Junginger, S. Kopp, K.K. Midha, V.P. Shah, S. Stavchansky, J.B. Dressman, Biowaiver monographs for immediate release solid oral dosage forms: Levofloxacin, J. Pharm. Sci. 100 (2011) 1628–1636.

[51] A. Kaur, D.B. Salunke, A. Umar, S.K. Mehta, A.S.K. Sinha, S.K. Kansal, Visible light driven photocatalytic degradation of fluoroquinolone levofloxacin drug using Ag₂O/TiO₂ quantum dots: a mechanistic study and degradation pathway, New J. Chem. 41 (2017) 12079–12090.

[52] X.-J. Wen, C.-G. Niu, H. Guo, L. Zhang, C. Liang, G.-M. Zeng, Photocatalytic degradation of levofloxacin by ternary Ag₂CO₃/CeO₂/AgBr photocatalyst under visible-light irradiation: Degradation pathways, mineralization ability, and an accelerated interfacial charge transfer process study, J. Catal. 358 (2018) 211–223.

[53] Q. Chen, Y. Xin, X. Zhu, Au-Pd nanoparticles-decorated TiO₂ nanobelts for photocatalytic degradation of antibiotic levofloxacin in aqueous solution, Electrochim. Acta 186 (2015) 34–42.

[54] M. Kaur, A. Umar, S.K. Mehta, S.K. Kansal, Reduced graphene oxide-CdS heterostructure: An efficient fluorescent probe for the sensing of Ag(I) and sunset yellow and a visible-light responsive photocatalyst for the degradation of levofloxacin drug in aqueous phase, Appl. Catal. B: Environ. 245 (2019) 143–158.